Investigation of electrically isolated capacitive sensing skins on concrete to reduce structure/sensor capacitive coupling

Emmanuel Ogunniyi[1] , **Alexander Vareen[1], Austin R J Downey[1,2],*** ,
Simon Laflamme[3,4] , **Jian Li[5]** , **Caroline Bennett[5]** , **William Collins[5], Hongki Jo[6],**
Alexander Henderson[2] and Paul Ziehl[1,2]

[1] Department of Mechanical Engineering, University of South Carolina, Columbia, SC, United States of America
[2] Department of Civil and Environmental Engineering, University of South Carolina, Columbia, SC, United States of America
[3] Department of Civil, Construction, and Environmental Engineering, Iowa State University, Ames, IA, United States of America
[4] Department of Electrical and Computer Engineering, Iowa State University, Ames, IA, United States of America
[5] Department of Civil, Environmental and Architectural Engineering, The University of Kansas, Lawrence, KS, United States of America
[6] Department of Civil, Architectural Engineering and Mechanics, The University of Arizona, Tucson, AZ,United States of America

E-mail: austindowney@sc.edu

CrossMark

Abstract

Damage to bridges can result in partial or complete structural failures, with fatal consequences. Cracks develop in concrete infrastructure from fatigue loading, vibrations, corrosion, or unforeseen structural displacement. Effective long-term monitoring of civil infrastructure can reduce the risk of structural failures and potentially reduce the cost and frequency of inspections. However, deploying structural health monitoring technologies for crack detection on bridges is expensive, especially long-term, due to the density of sensors required to detect, localize, and quantify cracks. Previous research on soft elastomeric capacitors (SECs) has shown their viability for low-cost monitoring of cracks in transportation infrastructure. However, when deployed on concrete for strain monitoring, a structure/sensor capacitive coupling exists that may cause a significant amplification in the signal collected from the SEC sensor. This work provides a detailed experimental study of electrically isolating capacitive sensing skins for concrete structures to reduce the structure/sensor capacitive coupling of an electrically grounded sensor. The study illustrates that the use of rubber isolators effectively

---

* Author to whom any correspondence should be addressed.

decreases the capacitive coupling between concrete, which inherently has capacitive properties, and sensors such as the SEC that utilize capacitance measurements. In addition, the required thickness of isolation for accurate strain monitoring using the SEC with geometry described in the paper is investigated and better strain correlation is observed between the rubber of isolation thickness 0.30 mm and 0.64 mm with rubber of isolation of approximately 0.40 mm having the best response. Tests were conducted on small-scale concrete beams, and results were validated on full-scale reinforced concrete bridge decks recently taken out of service. This study demonstrates that with proper isolation material, the SEC can accurately transduce strain from concrete within a 10 $\mu\varepsilon$ error for strain levels beyond 25 $\mu\varepsilon$.

(Some figures may appear in colour only in the online journal)

1. Introduction

The deployment of structural health monitoring (SHM) technologies on bridges can be costly because numerous sensors are typically needed to gather a meaningful dataset across large surface areas. Moreover, geometrically complex structural details can be difficult to monitor with available sensing devices [1]. Smart sensing skins have been advantageous for continuous sensing over large areas [2–4], including surface sensors based on photonic crystals [5], carbon nanotube sensing skins [6, 7], damage sensitive paints [8], self-sensitive materials [9, 10], etc. Construction of *smart bridges* that incorporate particular sensors like strain gauge, corrosion sensors, and fiber-optic sensors [11] during construction is one of the most recent developments in SHM for bridges. However, the precision of these sensors may be constrained by environmental conditions such as humidity, wind, temperature, solar radiation, and on-site construction defects at the job site [1].

The soft elastomeric capacitor (SEC) is a sensing skin developed for mesoscale sensing that has been used both for fatigue crack detection in steel structures [2] and the reconstruction of full-field strain maps in structures [12]. Its relative cost, durability, and flexibility have made it a suitable sensor for large-area surface monitoring [13]. The SEC is a capacitive sensor attached to the structure being monitored with a thin layer of off-the-shelf epoxy. In-plane deformation in the structure (i.e. strain) produces a change in capacitance on the SEC. Changes in capacitance can be used to infer the structure's functionality when monitored over time. The strain on the monitored surface is obtained through the strain-capacitance relationship described in the electromechanical model of the SEC [2]. Of importance to this work are previous studies on the use of SEC for crack monitoring and detection; studies that investigate the use of SEC as strain sensing sheets on steel plates for crack detection report progressive data over the recent years [14]. The studies have also been extended to strain sensing on concrete [15, 16].

Investigations on the concrete show that the SEC is sensitive to localized cracks on the concrete substrate [15]. However, strain values measured by the SEC are higher than the actual strain on the concrete being monitored. In order to utilize the SECs on concrete structures, it is essential to measure the actual strain present in the concrete, as opposed to simply monitoring abnormal variations (such as those caused by damage). In this work, it is hypothesized that high strains recorded by the SECs bonded on the concrete surface result from capacitance coupling between the SEC/concrete interface due to the intrinsic capacitance of the cement matrix in the concrete. [17]. Therefore, the challenge with deploying SECs on concrete is not because of the slight electrical conductivity of the concrete but rather its intrinsic capacitance. For example, the SEC has been successfully deployed on conductive materials such as aluminum and steel. The success of the SEC on conductive materials is attributable to the fact that the impedance of these materials is nearly perfectly resistive. At the same time, concrete has a significant capacitive component to its impedance.

The authors introduce rubber as an isolation material between the SEC/concrete interface in this paper. Here, the thin rubber isolator eliminates unwanted electrical interference from the concrete on the SEC while allowing high-strain transmissibility. The contributions of this work are (a) extending previous research efforts on strain sensing on concrete by reducing capacitance coupling between the SEC and concrete using a rubber isolator, (b) investigating the performance of the SEC at different strain levels on concrete, and (c) providing an experimental investigation on capacitive coupling between a sensing skin and concrete structure. The paper is organized as follows. First, section 2 presents a background to the current study, including the SEC properties and electromechanical model of the SEC. Next, section 3 expounds on the methodology, and the subsequent sections discuss the results and conclude the paper.

2. Background

2.1. SECs

The SEC is fabricated from a styrene-block-ethylene-co-butylene-block-styrene (SEBS) matrix where the sensor's dielectric is filled with titania (TiO_2) while its electrodes are doped with carbon black (CB) particles to make a conductive polymer. The manufacturing steps of the SEC are described in detail in prior work [18]. The SEC is a SEBS matrix, either filled or doped with additives to make a capacitor; the layers
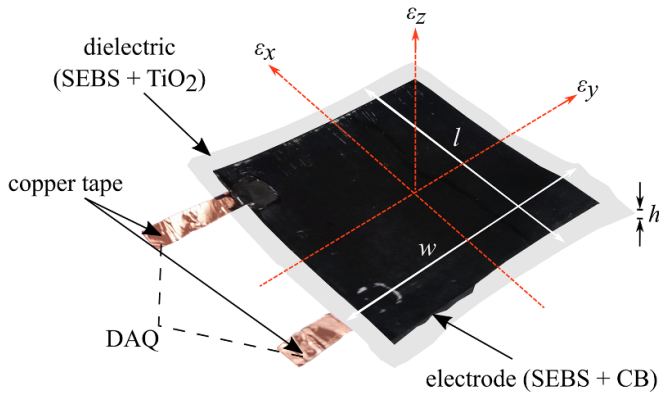
Figure 1. Sensing principle for a single SEC showing the schematic of the SEC including the dimensions and strain direction as measured by the SEC.

that make up the SEC have a robust mechanical connection since the electrodes and dielectric is made of the same polymer matrix (SEBS). In addition, the SEC's long-term weatherability has been demonstrated [19], making it an excellent candidate for long-term and low-cost monitoring of mesoscale structures. Figure 1 shows the schematic of a single SEC with a surface area of 76.2×76.2 mm (3×3 in). It is worth noting that the geometry (such as form and size) can be changed. The resulting sensor has the following features: low cost, highly elastic, mechanical robustness, ease of installation, and low power consumption.

2.2. Electromechanical model

The SEC measures strain induced by deformations from the surface monitored. Deformations on the SEC result in an equivalent change in capacitance. Therefore, the SEC can be modeled as a parallel plate capacitor with the relationship in equation (1).

$$C = e_0 e_r \frac{A}{h} \qquad (1)$$

where $e_0 = 8.854 \mathrm{pF\,m^{-1}}$ is the vacuum permittivity, e_r is the dimensionless polymer relative permittivity, h is the thickness of the dielectric, and $A = l \cdot w$ is the sensor area where w is the width and l is the length as shown in figure 1. Changes in capacitance, ΔC, can be obtained by differentiating equation (1) (assuming small changes in strains on the monitored surface):

$$\frac{\Delta C}{C_0} = \left(\frac{\Delta l}{l_0} + \frac{\Delta w}{w_0} - \frac{\Delta h}{h_0} \right) = \varepsilon_x + \varepsilon_y - \varepsilon_z \qquad (2)$$

ΔC denotes the capacitance change of the SEC due to strain, and C_0 represents the initial value of the SEC capacitance. ε_x, ε_y and ε_z are strains in the x, y and z directions, respectively. The SEC is deployed in the $x - y$ plane for surface strain monitoring. Assuming plane stress and applying Hooke's law,

$$\varepsilon_z = -\frac{\nu}{1-\nu}(\varepsilon_x + \varepsilon_y). \qquad (3)$$

By substituting equations (3) into (2), a free-standing SEC has a capacitance response as,

$$\frac{\Delta C}{C_0} = \frac{1}{1-\nu_0}(\varepsilon_x + \varepsilon_y) \qquad (4)$$

$$\frac{\Delta C}{C_0} = \lambda_0(\varepsilon_x + \varepsilon_y) \qquad (5)$$

where ν_0 is Poisson's ratio for the SEC, and λ_0 is the SEC's gauge factor

In this paper, a gauge factor of 1.7 was used, experimentally validated in Liu *et al* [20]. If ε_m is the strain on the monitored surface:

$$\varepsilon_m = (\varepsilon_x + \varepsilon_y) \qquad (6)$$

$$\frac{\Delta C}{C_0} = 1.7(\varepsilon_x + \varepsilon_y) \qquad (7)$$

$$\frac{\Delta C}{1.7C_0} = \varepsilon_m \qquad (8)$$

equation (8) presents the relationship between nominal surface strain which is the measure of the deformation of the concrete specimen caused by an applied load; in this case, defined as the change in the length of the concrete divided by its original length and measured capacitance changes on SEC that can be used in structural monitoring.

2.3. Challenges associated with strain sensing on concrete

Strain sensing on concrete is associated with several inherent mechanical and electrical challenges. First, there are mechanical challenges with sensing strain on concrete due to its uneven, rough, and porous surfaces, resulting in issues when installing strain gauges on the surface. As a result, special preparations are required to ensure that strain on irregular concrete surfaces is fully transferred to strain gauges [21]. Furthermore, concrete is a heterogeneous material; the several components making up its structure can lead to the localization of stress and strain during loading, which can be a challenge when sensing strain with small sensors. However, the SEC's large size and simple installation process are sensor attributes well-suited for monitoring concrete.

Electrical challenges associated with SECs on concrete have been previously noted. For example, experimental results from Yan *et al* [15] show that when an SEC sensor is attached to concrete, the measured strain values are significantly higher than anticipated. However, results by Yan *et al* [15], and Downey *et al* [16] show that when the exact amplitude of the signal is not considered significant but only the response to loading and damages is monitored, the general functionality of the SEC is not affected when used on concrete. The detection of crack formation can be inferred by monitoring an increase in the capacitance change of the SEC. Moreover, work by Laflamme *et al* [18] has shown that the SEC can accurately transduce the dynamic signals in a modal

test of a reinforced concrete beam. However, accurate strain monitoring of concrete using the SEC has not yet been demonstrated due to 'amplification' in the SEC signal when attached directly to concrete. It is hypothesized that the amplification of the SEC's signal when adhered directly to the concrete is due to a complex capacitive coupling between the SEC and the intrinsic capacitance of the concrete. This hypothesis is tested throughout this work.

Several changes are expected to be seen as concrete undergoes mechanical deformations, including changes in intrinsic resistivity, change in bonding between the fillers and cement matrix, and change in capacitance [22–24]. These resulting changes pose challenges to external sensors attached directly to the concrete surface or inside the concrete. In particular, a few studies have demonstrated the intrinsic capacitance of concrete and how it varies with strain [23, 24]. For example, in concrete, capacitance-based strain sensing is based on piezo-permittivity in which the permittivity of concrete increases upon compression, and vice versa under tension [23]. This can result in a 2%–9% change in the capacitance of the measured concrete [24], which is hypothesized to interact with any capacitive-based sensors (i.e. SEC) mounted on the surface of the concrete.

Moreover, an investigation by Cheng *et al* [25] detail how the size, position, and depth of rebar in the reinforced concrete beam affects the capacitance value recorded by a surface-mounted capacitance transducer. In addition, their results show that the corrosion of steel reinforcement affects capacitance values. Hence, using surface-mounted capacitance sensors like SECs to measure strain potentially faces challenges related to capacitive coupling.

3. Methodology

This section discusses the experimental procedure and materials for evaluation of the SEC for strain sensing on concrete.

3.1. Electrical isolation material

Natural rubber and neoprene with a durometer of 40 A were selected as rubber isolators to investigate the SEC and concrete capacitance isolation. These two rubber isolators were selected because their Poisson ratios are close to 0.5, similar to SEC's Poisson ratio. Supplier-provided material properties are shown in table 1. Multiple thicknesses of the rubber isolators were investigated to determine the most efficient thickness of the rubber isolator that accurately described strain on the concrete specimen. For natural rubber, thicknesses of 0.203, 0.254, 0.305, 0.356, 0.508, 0.635, and 0.762 mm were investigated; for neoprene, 0.397, 0.793, 1.59, and 2.38 mm thickness were investigated. The installation of the rubber isolator to the concrete was done using a thin layer of off-the-shelf bi-component epoxy (JB Weld) to adhere it to the surface of the concrete before proceeding to install the SEC on the rubber isolator with the same epoxy.

A schematic representation of the SEC for strain sensing on concrete without an isolation layer between the SEC and

Table 1. Table showing rubber properties for natural rubber and neoprene.

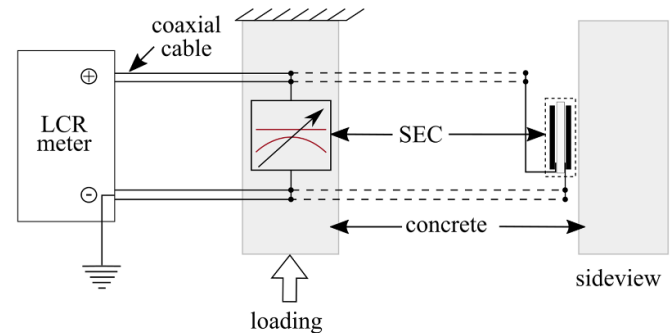| Properties	Natural rubber	Neoprene
Durometer or hardness range	40 A	40 A
Poisson's ratio	0.48–0.5	0.46–0.49
Tensile strength range	(≥ 17237 kN m^{-2})	5516–9653 kN m^{-2}
Elongation (range %)	300–900%	100–800%
Temperature range	93.3–200 °C	−34.4–121.1 °C

Figure 2. Circuit representation of the SEC as a variable capacitor adhered to the concrete sample with connection details.

concrete is shown in figure 2: the SEC is represented as a variable capacitor adhered to the concrete surface. The connection to the SEC's conductive plate attached directly to the concrete is grounded. However, this grounding does not reduce the structure/sensor capacitive coupling. As mentioned in the introduction, the overestimated strain signal obtained during testing led to further investigations on using rubber isolators between the SEC and concrete surfaces for capacitance decoupling.

Figure 3 reports the schematic representation of the strain transfer mechanism between the SEC and rubber isolator on the compressively loaded concrete specimen. The epoxy/bonding layers are thin and have a similar stiffness to the concrete, so their significance in the strain transfer mechanism can be ignored. The thickness of the rubber is denoted as *t*, and it is varied through the experimental process presented in this work. During the loading process, compressive strain in the concrete is transferred to the rubber isolator and then to the SEC. A thin layer of off-the-shelf epoxy is used to adhere the SEC to the rubber isolator as depicted in figure 3(b). This thin layer ensures that any variations in the rubber isolator are directly transmitted to the SEC. However, strain transmissibility from the concrete to the SEC through the rubber isolator depends on the thickness of the rubber and is explored in this work. Figure 3(c) shows the rubber isolator in a deformed state. It is hypothesized that as the thickness *t* of the rubber isolator increase or decreases, *d* increases or decreases.

3.2. Data acquisition and processing

Capacitance data from the SEC were collected using an LCR meter (BK precision 891) with a driving frequency of 1 kHz,
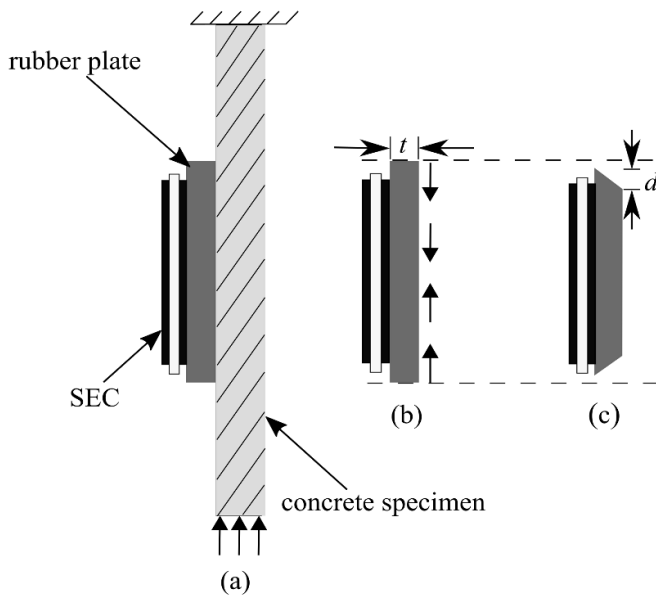
Figure 3. Deformation of the rubber isolating layer under a compression load showing: (a) diagram of the SEC and rubber isolator on the concrete surface; (b) SEC and rubber isolator without deformation with the arrows showing the strain direction, and; (c) SEC and rubber isolator after deformation.

with a LabVIEW code to control the data acquisition process. The acquired capacitance data is related to strain according to the electromechanical model described in section 2. Data from a reusable surface-mount resistance bridge-based strain transducer (model ST350 manufactured by BDI) was acquired using a Bridge Analog Input (NI-9237 manufactured by NI). This reusable surface-mounted strain transducer is referred to as a 'strain transducer' throughout this work. Load and displacement were acquired directly from the dynamic testing machine using an analog digitizer (NI-9239 manufactured by NI).

3.3. Testing procedure

Figure 4 shows the experimental setup used in this paper to investigate the concrete samples. Figure 4(a) shows a dynamic testing machine (MTS with Model No. 609.25A-01), having a maximum loading capacity of 250 kN. Compression tests were carried out to measure the SEC's compressive strain on a concrete specimen.

The concrete specimen is an unreinforced concrete section, with dimensions $0.305 \times 0.102 \times 0.102$ m ($4 \times 4 \times 12$ in). The concrete was made using a 27 MPa (4000 psi) strength concrete mix, 3.5 L of water per 36.3 kg (80 lb) of concrete mix, and has an approximate density of 2014 kg m^{-3} (125.73 lb ft^{-3}) on each sample. The specimens were allowed to cure for at least seven days before testing since only strain is acquired during the test, and the strength of specimens is not of priority. No changes in the concrete/sensor capacitive coupling were noticed with specimens allowed to cure for up to 6 months [15, 16]. In the exploratory stage of this study, more than 50 samples of concrete specimens were tested. To ensure consistency in the data, experimental trials were repeated at

various intervals of concrete curing with varying levels of humidity and grounding and shielding. However, the problem of capacitive coupling persisted in all test cases.

The cyclic loading procedure was designed to evaluate the performance of the SEC as a strain-sensing material on the concrete specimen, as shown in figure 5. The cyclic load was a 0.05 Hz harmonic excitation in fixed-compression mode between -22.5 and -45 kN. Strain data on the specimen-scale sample were obtained from the concrete using the SEC, strain transducer, and digital image correlation (DIC) during a steady-state cyclic loading condition. The concrete specimen was pre-loaded to -45 kN before strain data was acquired to prevent signal drift that is recorded during the initial loading. A drift in the SEC's signal was observed when the concrete specimen was initially loaded from a rest state, believed to be caused by electrical interference with the dynamic testing machine and in the initial settling of the concrete specimen under load. To compensate for this drift, the compression loading was started from a compressed state of -45 kN, as shown in figure 5.

The SEC and rubber isolator adhered to the surface of the concrete using the before-mentioned off-the-shelf bi-component epoxy after it was cleaned with sandpaper. During installation, the SEC was stretched slightly on all sides, of which the applied stretch to the SEC is about 2% of the original dimension on all sides to create initial strain on the SEC, allowing it to deform with the specimen. SEC installation on the full-scale concrete deck followed the same procedure. A coaxial cable was used to connect the copper tapes on the SEC to the data acquisition system for capacitance data acquisition. Special care is taken in cable management to ensure the cables do not move during testing.

Figure 6 shows the DIC setup used to observe the strain on the surface of the SEC, where the image focus and area of interest for strain evaluation are set on the SEC. This is done to compare the strain undergone by the SEC to the one measured directly by the SEC. In this work, a 5 MP camera controlled using VIC-snap from correlated solutions was used, and data were processed through VIC-3D. Strain data from the SEC, strain transducer, and DIC were obtained simultaneously using the previously described acquisition systems for each sensor. The results from the DIC measurements were also compared to the reference strain transducer measured values. For the DIC measurements, only the strain in the vertical direction ε_y, is considered for data processing.

3.4. Full-scale bridge deck evaluation

Experiments on the full-scale reinforced concrete bridge deck were performed to mimic an actual bridge's strain measurement. Figure 7 shows the setup for three-point bending of a full-scale reinforced concrete bridge deck with dimensions $4.27 \times 1.52 \times 0.23$ m. This panel was removed from an in-service bridge deck and used to validate the SEC for monitoring strain on a real-world concrete structure. The loads introduced to the deck were controlled using a Shore-Western hydraulic actuator. These unordered loads were applied to demonstrate the SEC response on a full-scale structure in
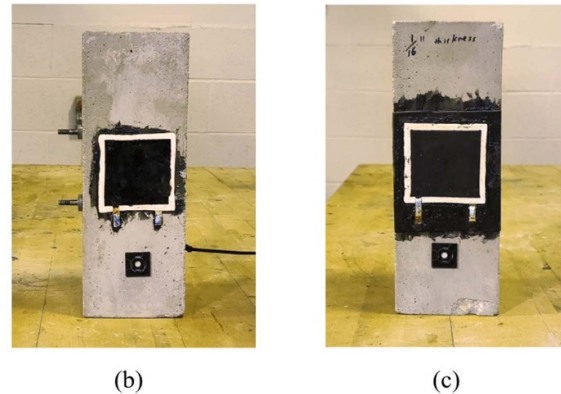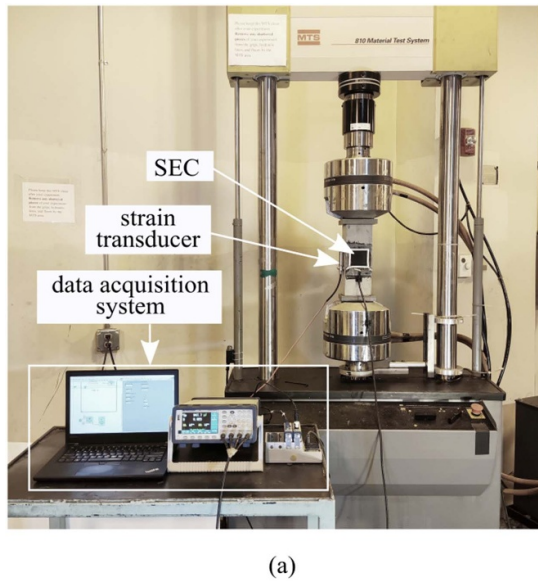
Figure 4. The specimen-scale testing experimental setup showing: (a) the concrete specimen on the dynamic testing system (MTS) with the data acquisition system which includes the NI DAQ and BK Precision 891 300 kHz; (b) the concrete specimen with SEC without isolation, and; (c) the concrete specimen with SEC with rubber isolator.
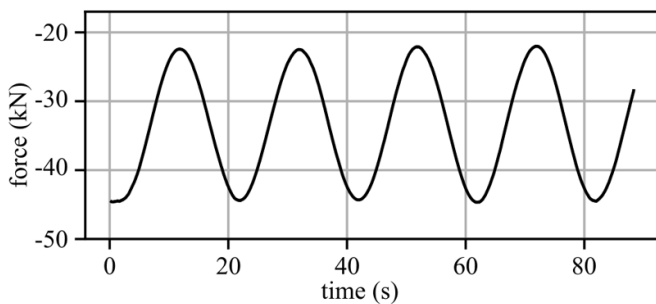

Figure 5. Loading profile for the concrete specimen showing the cyclic load between −22.5 kN and −45 kN.
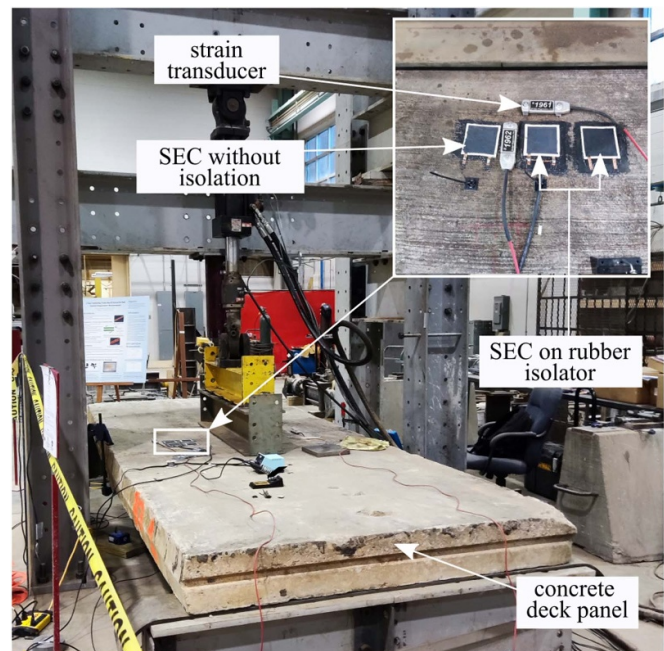

Figure 6. DIC experimental setup for strain data collection on the speckled concrete specimen.

Figure 7. Experimental setup for full-scale reinforced concrete deck panel.

during installation. The SEC and reference strain transducer were placed side by side at the center of the deck, where maximum strain is expected to be observed as shown in the inset of figure 7.

4. Results and discussion

This section explores the examination of several experimental trials that are conducted to assess the strain-sensing abilities
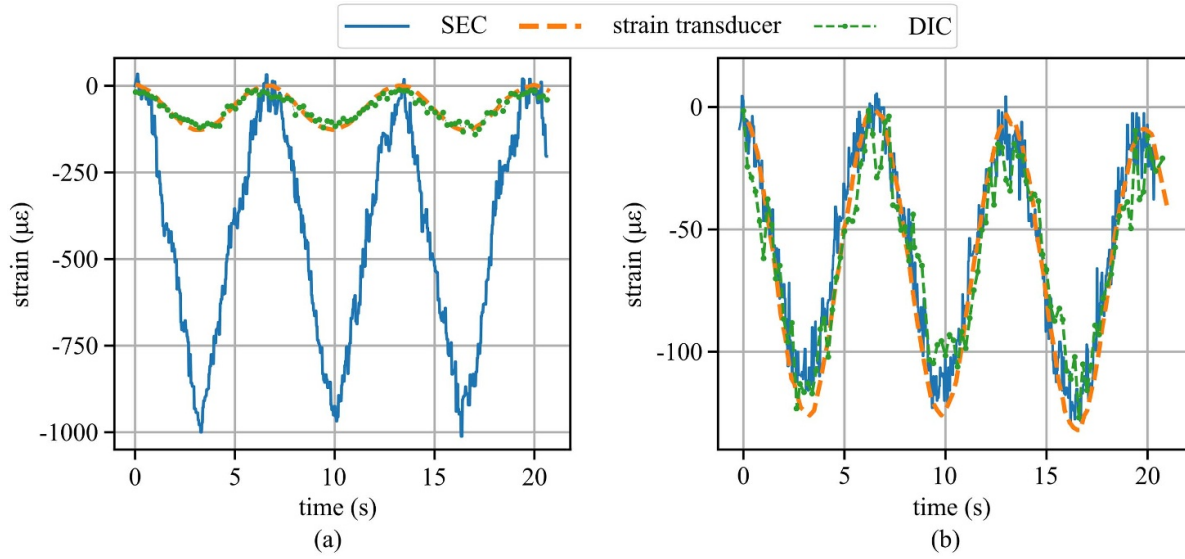
the electrically noisy environment of a structures lab, simulating real-world conditions on a bridge. The SECs were installed on the bridge deck similarly to the small concrete specimens, and the same stretch of about 2% was applied

Figure 8. Strain results from SEC, strain transducer, and digital image correlation on (a) SEC adhered directly to concrete, showing the amplification of the SEC strain signal over the reference measurements; and (b) SEC signal using isolation with a rubber isolator of 0.397 mm thick.

of the SEC and the effectiveness of electrical isolators when used on concrete specimens.

The decibel signal-to-noise ratio (SNR_{db}) and mean absolute error (MAE) from the data observed are calculated using equations (9) and (10), where z in equation (10) is the total number of samples collected. These calculations are used to determine the acceptability of the proposed use of a rubber isolator with SEC,

$$SNR_{dB} = 10 \log_{10} \left(\frac{P_{signal}}{P_{noise}} \right) \qquad (9)$$

$$MEA = \frac{\sum_{i=1}^{z} |x_{true_i} - x_{est_i}|}{z}. \qquad (10)$$

4.1. Small-scale concrete specimens

4.1.1. Isolation of concrete specimen.
Strain data from the compression tests show that the SEC measures a higher strain than the strain measured by the reference strain transducer. This disparity in results where the SEC overestimates the strain in the concrete was repeatable and aligned well with data seen in prior research when the SEC was directly adhered to the concrete. The figure 8(a) displays the strain signal that has been amplified by the SEC. It is worth noting that the strain measurement obtained by the SEC closely aligns with the two widely used methods, DIC and strain transducer, in figure 8(b).

To study the effects using different capacitance measurement techniques, strain data were collected using two additional DAQs, both previously used successfully with the SEC. One DAQ was based on the PCAP02 capacitance-to-digital converter, which uses a time-constant measurement approach coupled with a time-to-digital converter [26]. Another was based on the FDC1004 capacitance-to-digital converter that uses a step waveform to excite the sensor and a sigma-delta

analog-to-digital converter [27]. Results from both systems were the same as that observed with the BK Precision 891 LCR meter. The results support the hypothesis that the SEC/concrete capacitance coupling affects the SEC's strain sensing capacities, hence the need to isolate the two surfaces.

Figure 8(b) reports SEC strain data obtained using a 0.397 mm thick rubber isolator with the SEC. Strain data were also acquired using a strain transducer and DIC. The data display a close correlation between the SEC, strain transducer, and DIC measurement, showing about 96% SEC strain accuracy when compared to the strain transducer, and about 94% accuracy when compared to the DIC measured data. In addition, the signal amplification observed in the test without isolation was eliminated, showing how a capacitive sensor's isolation enabled accurate strain monitoring on concrete.

4.1.2. DIC investigation of strain on the surface of SEC without isolation.
DIC was used to investigate strain transmissibility through the SEC by investigating strain on the outer surface of the SEC adhered to the concrete. The DIC investigation was done using the experimental setup shown in figure 6 by loading the concrete specimen with the described cyclic loading procedure. This study was done on the first 3 s of figure 8(a), where strain rises from 0 to -110 $\mu\varepsilon$ over 3.03 s.

The DIC strain data are shown in figure 9, where the distributed strain along the y-axis (ε_y) on the surface of the SEC is shown from (a) to (f). Incremental strain is referenced from figure 9(a), therefore showing no strain at time 0 s. Figures 9(b)–(f) report strain data at equal time intervals of 0.6 s. A tensile strain of less than 25 $\mu\epsilon$ can be observed on the surface of SEC in figure 9(b). The unevenness of the concrete causes this strain. As loading increases, the compressive strain becomes more prevalent.

Figure 9(f) shows the maximum strain recorded using the DIC. Note that the strain is not evenly distributed. However,
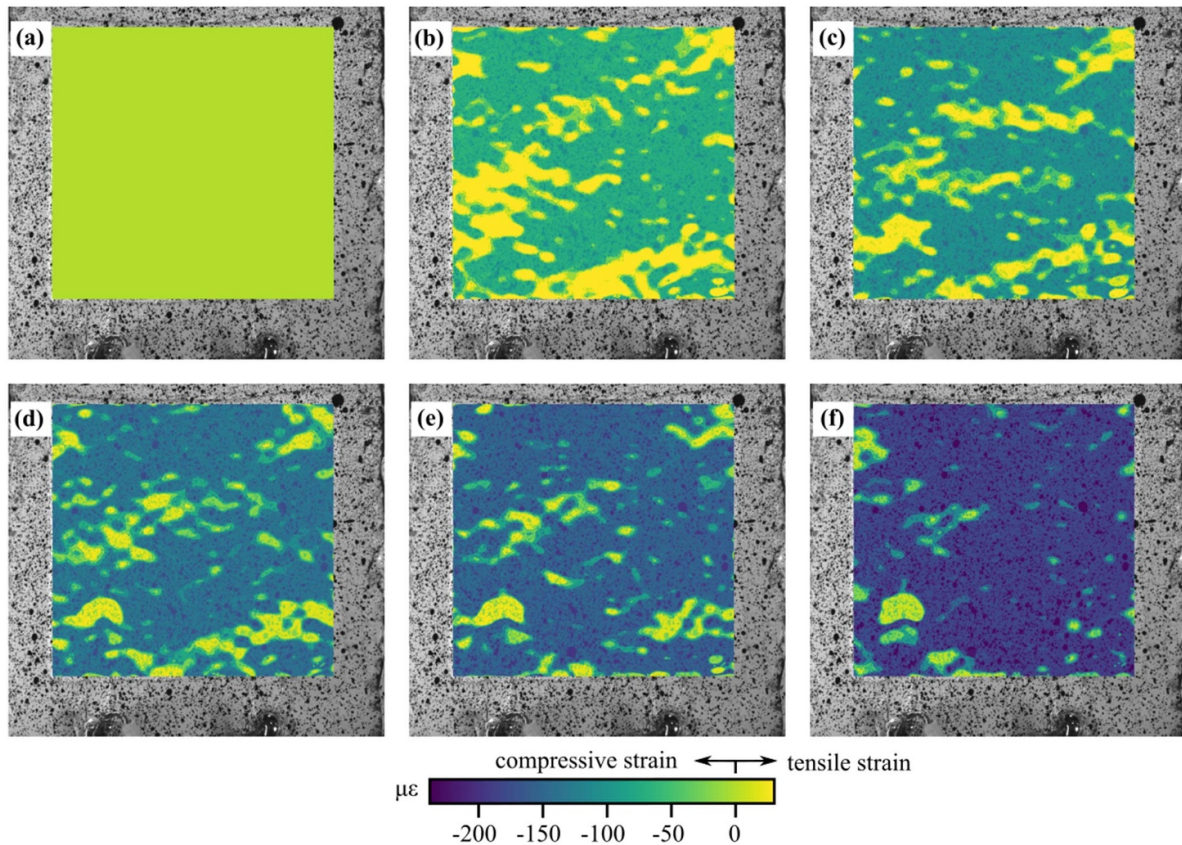
Figure 9. DIC measured surface strain in the SEC adhered to concrete without isolation under the loading shown in figure 8(a) at a specific time considered with: (a) at 0 s with a nominal strain value of 0 $\mu\varepsilon$; (b) 0.63 s with a nominal strain value of -25.4 μ, (c) 1.23 s with a nominal strain value of -57.7 μ, (e) 1.83 s with a nominal strain value of -87.1 $\mu\varepsilon$, and; (e) 2.43 s with a nominal strain value of -96.6 $\mu\varepsilon$, and; (f) 3.03 s with a nominal strain value of -110.1 $\mu\varepsilon$, where the color bar indicates the strain at each point on the outer surface of the SEC with point 0 to the negative being compressive strain and 0 towards positive representing tensile strain.

Table 2. Strain data on concrete obtained from SEC, strain transducer, and DIC without isolation in the first 3.03 s of figure 8(a).

time (s)	SEC ($\mu\varepsilon$)	strain transducer ($\mu\varepsilon$)	DIC ($\mu\varepsilon$)
0	0	0	0
0.63	-37.6	-17.9	-25.4
1.23	-247.6	-52.8	-57.7
1.83	-421.1	-86.9	-87.1
2.43	-684.2	-115.2	-96.6
3.03	-1004	-126.9	-110.1

the overall sum of the strain on the concrete is compressive at -110 $\mu\varepsilon$, compared to the SEC reported strain which is -1004 $\mu\varepsilon$ at the same time of 3.03 s. Table 2 details the strain measurements by the SEC, strain transducer, and DIC between 0 and 3.03 s. Table 2 confirms that the strains measured by the strain transducer and DIC agree, while the SEC sensor overreports the strain.

4.1.3. Experimental testing of different isolation thickness. A study on the effects of the thickness of the rubber isolator is carried out to investigate the behavior of the SEC with

different rubber isolator thicknesses for accurate strain sensing. Figures 10(a)–(k) reports the strain results with the use of different rubber isolator thicknesses, from 0.203 to 2.381 mm.

As the thickness of the rubber isolator increased to 0.305 mm figure 10(c), SEC and strain transducer data became better matched. However, the correlation began to decrease again after figure 10(g) with a rubber isolator of thickness 0.635 mm. Better strain correlation is observed between figure 10(c) at 0.305 mm to figure 10(g) at 0.635 mm, with each measured thickness having a high SNR of at least 25. Furthermore, the SNRs presented in figure 11 shows that a rubber isolator with a thickness of 0.397 mm has the highest SNR. The MAE is another metric used to assess the effectiveness of isolation thickness. The rubber thickness of 0.397 mm has a lower MAE than other rubber insulators. These results support the hypothesis that adding the proper thickness of the isolation layer between the concrete and SEC decouples the capacitive interactions. However, the strain transmissibility through the electrical isolator becomes the limiting factor with increasing thickness.

4.1.4. Strain range test with SEC on concrete. As reported in previous work, the SEC is best suited for 25 $\mu\varepsilon$ and above strain measurements. This is due to the relatively high noise
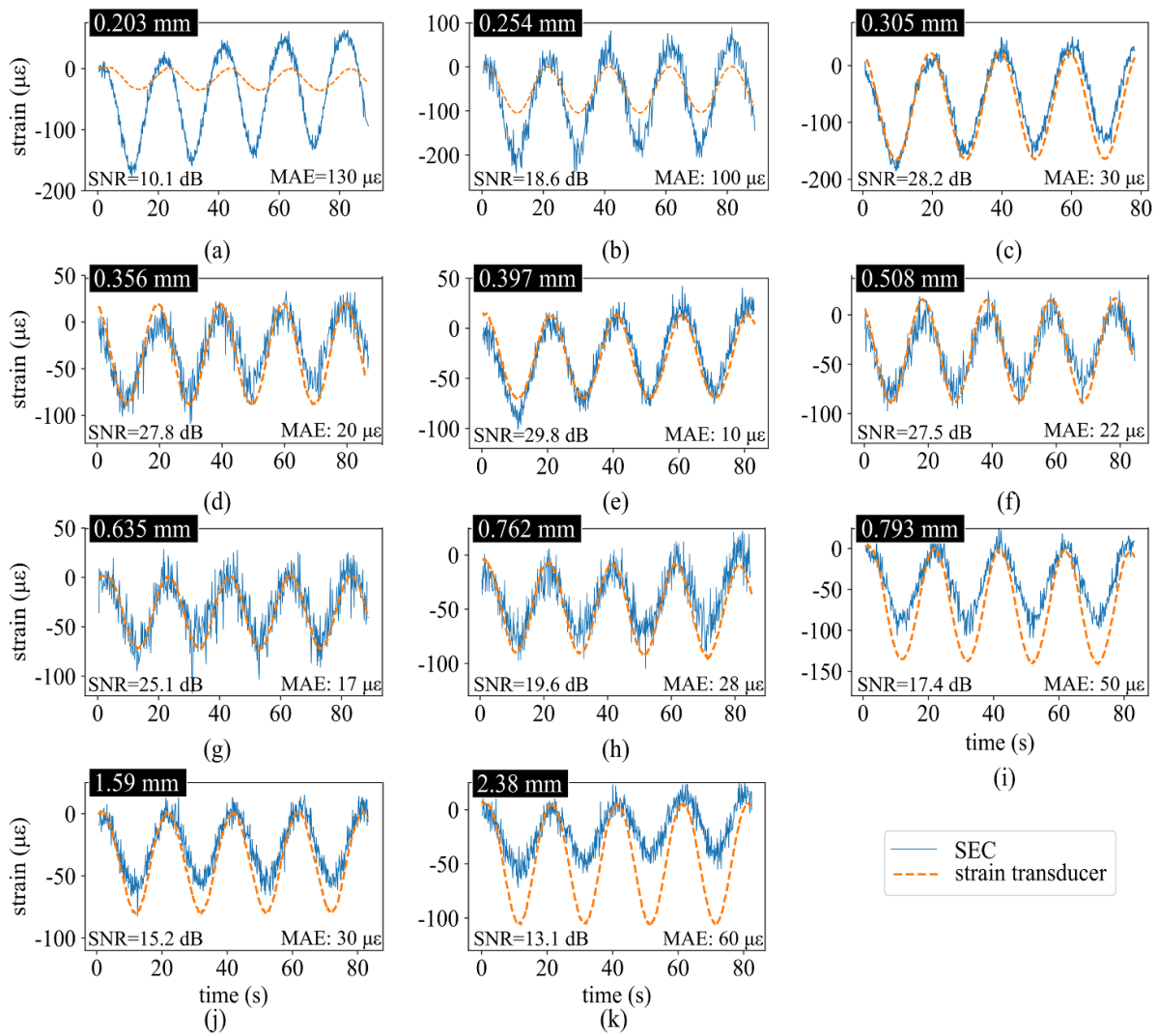
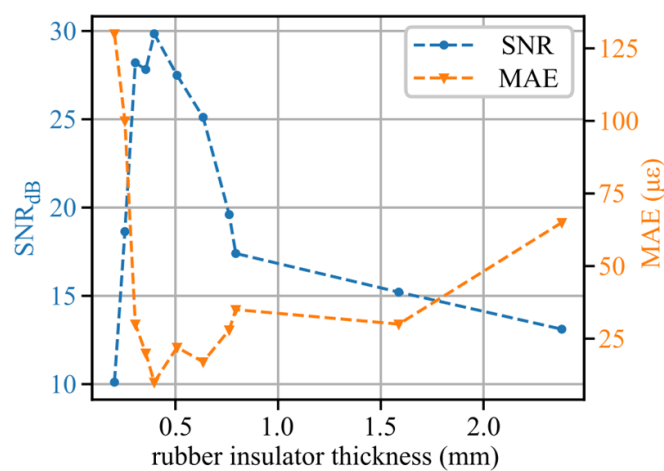**Figure 10.** Strain data from use of different rubber isolator thickness for SEC/concrete isolation.

Figure 11. Signal to noise ratio of strain data of rubber isolator with varying thickness.

in the measured signal. Figure 12 shows the strain measured by the SEC alongside the 0.397 mm rubber isolator and strain transducer as applied loading (strain level) was reduced. In this test, a rubber isolator with a thickness of 0.397 mm was chosen for use due to its superior performance in terms of SNR and lower MAE when compared to other rubber isolators that were
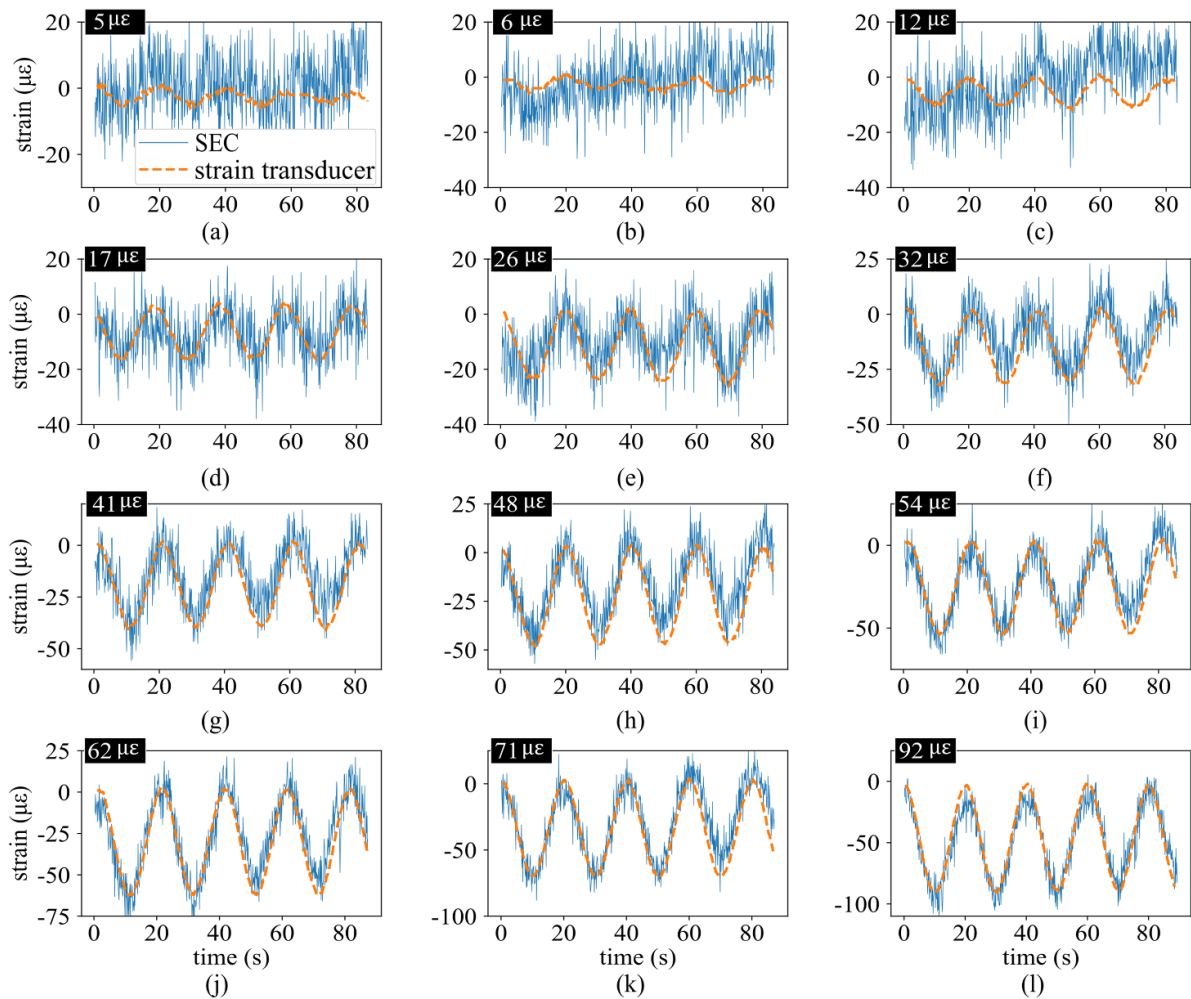
Figure 12. SEC Strain measurement obtained with a 0.397 mm rubber isolator for strain levels between 5 με and 92 με.

evaluated. As shown, strain levels above approximately 25 με can be accurately measured by the SEC. However, strain below 25 με was affected by noise and will require a digital filter to digitize strain data from the SEC accurately. Note that the SEC can stretch up to 500% its original length in an unbounded configuration. Therefore, upper strain measurement in tension is limited by the concrete substrate, while its limit in compression strain measurement is limited by pre-tension applied to the SEC during installation on the structure.

Figure 13 reports the error in strain data from the SEC when compared to the reference strain data from the strain transducer. As indicated in the error plot, the clarity in the sensed strain is reduced at strain below 25 με. Therefore, using the SEC for sensing strain at 25 με and above on concrete surfaces is advisable. Results are consistent with the 25 με accuracy reported in previous work [13].

Figure 13. Percentage error for strain sensing at different strain levels with SEC.

4.2. Full-scale testing

For the full-scale reinforced concrete deck panel test shown in figure 7, two rubber isolators of thicknesses 0.397 and 0.793 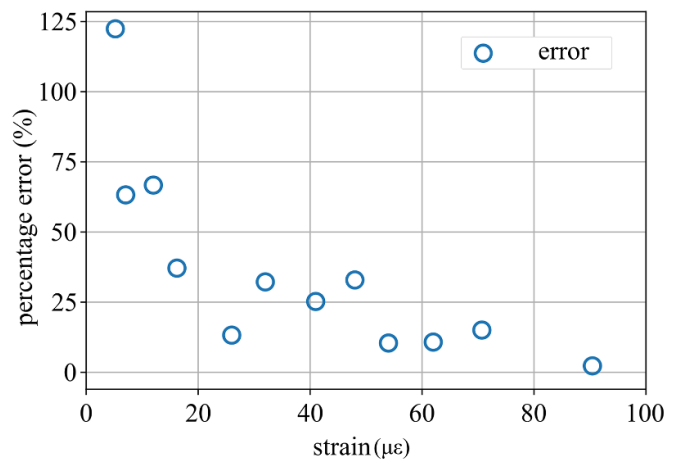mm were tested. 0.397 mm was chosen due to its good SNR demonstrated in the previous test in section 4.1, and 0.793 mm to show how a thicker isolation material affects strain sensing with the SEC. The SECs adhered to these two rubber isolators are investigated alongside an SEC directly
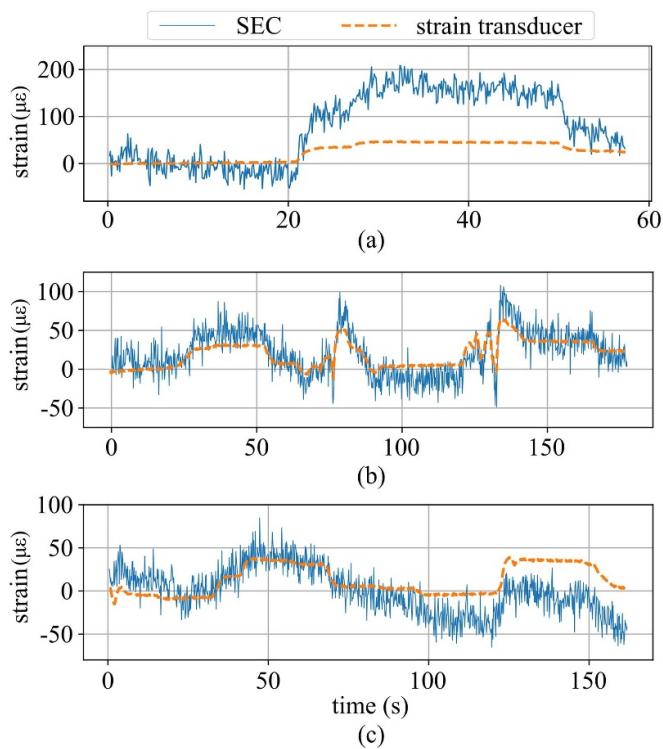
Figure 14. Strain data on full-scale reinforced concrete; (a) without rubber isolator; (b) with rubber isolator of thickness 0.397 mm, and; (c) with rubber isolator of thickness 0.794 mm.

adhered to the surface of the reinforced concrete deck panel to measure strain data, as shown in the inset of figure 7. Two strain transducers were placed on the bridge deck to measure both horizontal and vertical strains, which, when combined, provide a total strain measurement by the strain transducer.

Figure 14 reports the temporal results for the full-scale test. Figure 14(a) reports the data for an SEC with no rubber isolator, and as expected, the SEC measured a higher strain value when compared to the strain transducer.

With the addition of a rubber isolator of thickness 0.397 mm, shown in figure 14(b), the SEC signal better aligns with that measured by the strain transducer. A similar result is observed in figure 14(c), where the rubber isolator of thickness 0.794 mm is used. In figure 14(c), a slight drift in the sensor signal is noticed after 80 s. However, the strain measured by the SEC is still better correlated with that from the strain transducer than the strain measured from the SEC directly adhered to the concrete. The result shows that a similar strain trend in the small-scale concrete sample is repeatable in full-scale reinforced concrete.

5. Conclusion

Using a SEC sensor (SEC), the study investigated strain sensing on concrete by introducing isolation materials at the SEC/-concrete interface. Initial investigations show the need for an isolation material in the SEC/concrete interface for accurate strain measurement. This is because of the hypothesized

capacitance coupling between the SEC and concrete, which results in an overestimated strain by the SEC. The use of isolation material at the SEC/concrete interface was found to effectively decreases the capacitive coupling between the concrete the SEC

Experimental investigations used rubber isolators as an isolation material at the SEC/concrete interface, and obtained strain data are compared to data from off-the-shelf strain transducers. The isolation data obtained are validated using DIC. Strain measurements are repeated on a full-scale reinforced concrete deck panel to mimic an actual bridge component. The results from the investigation showed about 96% SEC strain accuracy with the use of a rubber isolator with approximately 0.4 mm thickness.

When compared to off-the-shelf strain transducers, the SECs offer the ability to continuously monitor (spatial and temporal) large concrete structures. While off-the-shelf strain transducers for concrete surfaces provide good measurement quality; they can be expensive and difficult to maintain. Importantly when compared to the SEC, they do not cover large areas and therefore require a large number of sensors to provide distributed coverage of large structures like bridges. In addition, they are more sensitive to issues with bonding and surface preparation due to the point-wise installation of the sensors.

Further investigations showed that the SEC is more suitable for measuring strain at 25 $\mu\varepsilon$ and above on concrete. These results compare well to previous research on using SECs to monitor strain on steel and composites. The investigations report improvement in strain data from the SEC and advise on the further development of the SEC for accurate strain sensing on concrete. Future research would investigate modifications to SEC to eliminate the need for isolation and the investigation of crack detection on concrete.

Data availability statement

The data that support the findings of this study are available upon reasonable request from the authors.

Acknowledgment

ORCID iDs

Emmanuel Ogunniyi ⓘ https://orcid.org/0000-0001-5456-5929
Austin R J Downey ⓘ https://orcid.org/0000-0002-5524-2416
Simon Laflamme ⓘ https://orcid.org/0000-0002-0601-9664
Jian Li ⓘ https://orcid.org/0000-0003-3439-7539
Caroline Bennett ⓘ https://orcid.org/0000-0002-2713-0011

References

[1] Alokita S, Rahul V, Jayakrishna K, Kar V, Rajesh M, Thirumalini S and Manikandan M 2019 Recent advances and trends in structural health monitoring *Structural Health Monitoring of Biocomposites, Fibre-Reinforced Composites and Hybrid Composites* (Amsterdam: Elsevier) pp 53–73

[2] Kharroub S, Laflamme S, Song C, Qiao D, Phares B and Li J 2015 Smart sensing skin for detection and localization of fatigue cracks *Smart Mater. Struct.* **24** 065004

[3] Tung S T, Yao Y and Glisic B 2014 Sensing sheet: the sensitivity of thin-film full-bridge strain sensors for crack detection and characterization *Meas. Sci. Technol.* **25** 075602

[4] Yao Y and Glisic B 2015 Sensing sheets: optimal arrangement of dense array of sensors for an improved probability of damage detection *Struct. Health Monit.* **14** 513–31

[5] Zonta D, Chiappini A, Chiasera A, Ferrari M, Pozzi M, Battisti L and Benedetti M 2009 Photonic crystals for monitoring fatigue phenomena in steel structures *proc. SPIE* **7292** 729215

[6] Loh K J, Hou T C, Lynch J P and Kotov N A 2009 Carbon nanotube sensing skins for spatial strain and impact damage identification *J. Nondestruct. Eval.* **28** 9–25

[7] Pyo S, Loh K J, Hou T-C, Jarva E and Lynch J P 2011 A wireless impedance analyzer for automated tomographic mapping of a nanoengineered sensing skin *Smart Struct. Syst.* **8** 139–55

[8] Withey P A, Vemuru V S M, Bachilo S M, Nagarajaiah S and Weisman R B 2012 Strain paint: noncontact strain measurement using single-walled carbon nanotube composite coatings *Nano Lett.* **12** 3497–500

[9] Hou T C and Lynch J P 2009 Electrical impedance tomographic methods for sensing strain fields and crack damage in cementitious structures *J. Intell. Mater. Syst. Struct.* **20** 1363–79

[10] Downey A, D'Alessandro A, Baquera M, García-Macías E, Rolfes D, Ubertini F, Laflamme S and Castro-Triguero R 2017 Damage detection, localization and quantification in conductive smart concrete structures using a resistor mesh model *Eng. Struct.* **148** 924–35

[11] Glišić B, Hubbell D, Sigurdardottir D H and Yao Y 2013 Damage detection and characterization using long-gauge and distributed fiber optic sensors *Opt. Eng., Bellingham* **52** 087101

[12] Sadoughi M, Downey A, Yan J, Hu C and Laflamme S 2018 Reconstruction of unidirectional strain maps via iterative signal fusion for mesoscale structures monitored by a sensing skin *Mech. Syst. Signal Process.* **112** 401–16

[13] Laflamme S, Saleem H S, Vasan B K, Geiger R L, Chen D, Kessler M R and Rajan K 2013 Soft elastomeric capacitor network for strain sensing over large surfaces *IEEE/ASME Trans. Mechatronics* **18** 1647–54

[14] Kong X, Li J, Bennett C, Collins W, Laflamme S and Jo H 2019 Thin-film sensor for fatigue crack sensing and monitoring in steel bridges under varying crack propagation rates and random traffic loads *J. Aerosp. Eng.* **32** 04018116

[15] Yan J, Downey A, Cancelli A, Laflamme S, Chen A, Li J and Ubertini F 2019 Concrete crack detection and monitoring using a capacitive dense sensor array *Sensors* **19** 1843

[16] Downey A R J, D'Alessandro A, Ubertini F and Laflamme S 2018 Crack detection in RC structural components using a collaborative data fusion approach based on smart concrete and large-area sensors *Proc. SPIE Int. Soc. Opt. Eng.* **10598** 105983B

[17] Wen S and Chung D D 2004 Electromagnetic interference shielding reaching 70 dB in steel fiber cement *Cem. Concr. Res.* **34** 329–32

[18] Laflamme S, Ubertini F, Saleem H, D'Alessandro A, Downey A, Ceylan H and Materazzi A L 2015 Dynamic characterization of a soft elastomeric capacitor for structural health monitoring *J. Struct. Eng.* **141** 04014186

[19] Downey A, Pisello A L, Fortunati E, Fabiani C, Luzi F, Torre L, Ubertini F and Laflamme S 2019 Durability and weatherability of a styrene-ethylene-butylene-styrene SEBS block copolymer-based sensing skin for civil infrastructure applications *Sens. Actuators* A **293** 269–80

[20] Liu H, Laflamme S, Li J, Bennett C, Collins W, Downey A, Ziehl P and Jo H 2021 Investigation of surface textured sensing skin for fatigue crack localization and quantification *Smart Mater. Struct.* **30** 105030

[21] Group M M V P Strain gage installations for concrete structures strain gages and instruments (available at: www. micro-measurements.com)

[22] Ding S, Dong S, Ashour A and Han B 2019 Development of sensing concrete: principles, properties and its applications *J. Appl. Phys.* **126** 241101

[23] Chung D 2021 Self-sensing concrete: from resistance-based sensing to capacitance-based sensing *Int. J. Smart Nano Mater.* **12** 1–19

[24] Chung D and Wang Y 2018 Capacitance-based stress self-sensing in cement paste without requiring any admixture *Cem. Concr. Compos.* **94** 255–63

[25] Cheng Y, Hanif A, Chen E, Ma G and Li Z 2018 Simulation of a novel capacitive sensor for rebar corrosion detectio *Constr. Build. Mater.* **174** 613–24

[26] Downey A, Sadoughi M, Laflamme S and Hu C 2018 Fusion of sensor geometry into additive strain fields measured with sensing skin *Smart Mater. Struct.* **27** 075033

[27] Kong X, Li J, Collins W, Bennett C, Laflamme S and Jo H 2018 Sensing distortion-induced fatigue cracks in steel bridges with capacitive skin sensor arrays *Smart Mater. Struct.* **27** 115008